Free vibration analysis of functionally graded shells by a higher-order shear deformation theory and radial basis functions collocation, accounting for through-the-thickness

# Free vibration analysis of functionally graded shells by a higher-order shear deformation theory and radial basis functions collocation, accounting for through-the-thickness deformations

A. M. A. Neves [a], A. J. M. Ferreira [b], E. Carrera [c], M. Cinefra [c], C. M. C. Roque [d], R. M. N. Jorge [a], C. M. M. Soares [e]

[a] *Departamento de Engenharia Mecânica, Faculdade de Engenharia, Universidade do Porto, Rua Dr. Roberto Frias, 4200-465 Porto, Portugal*

[b] *(Corresponding author: ferreira@fe.up.pt)*
*Departamento de Engenharia Mecânica, Faculdade de Engenharia, Universidade do Porto, Rua Dr. Roberto Frias, 4200-465 Porto, Portugal*

[c] *Departament of Aeronautics and Aerospace Engineering, Politecnico di Torino, Corso Duca degli Abruzzi, 24, 10129 Torino, Italy*

[d] *INEGI, Faculdade de Engenharia, Universidade do Porto, Rua Dr. Roberto Frias, 4200-465 Porto, Portugal*

[e] *Instituto Superior Técnico, Av. Rovisco Pais, Lisboa, Portugal*

**Abstract**

This paper deals with free vibration problems of functionally graded shells. The analysis is performed by radial basis functions collocation, according to a higher-order shear deformation theory that accounts for through-the-thickness deformation.

The equations of motion and the boundary conditions are obtained by Carrera's Unified Formulation resting upon the principle of virtual work, and further interpolated by collocation with radial basis functions.

Numerical results include spherical as well as cylindrical shell panels with all edges clamped or simply supported and demonstrate the accuracy of the present approach.

**Keywords:** functionally graded materials; shells; free vibration.

## 1 Introduction

Functionally graded materials (FGM) are a class of composite materials that were first proposed by Bever and Duwez [1] in 1972. In a typical FGM shell the material properties continuously vary over the thickness direction by mixing two different materials [2]. The computational modelling of FGM is an important tool to the understanding of the structures behavior, and has been the target of intense research [2–8]. The continuous development of new structural materials leads to ever increasingly complex structural designs that require careful analysis. Although analytical techniques are very important, the use of numerical methods to solve shell mathematical models of complex structures has become essential.

The most common numerical procedure for the analysis of the shells is the finite element method [9–13]. This paper considers collocation with radial basis fuctions as a meshless technique. A radial basis function, $\phi(\|x - x_j\|)$ depends on the Euclidian distance between distinct collocation points $x_{j,j} = 1, 2, ..., N \in \mathbb{R}^n$. The unsymmetrical Kansa method [14] is employed in this work, for its good accuracy and easy implementation. The use of radial basis function for the analysis of structures and materials has been previously studied [15–29]. The authors have applied the RBF collocation to the analysis of composite beams and plates [30–32]. The combination of CUF and meshless methods has been performed in [33–36] for laminated plates, in [37,38] for laminated shells, and in [39,40] for FGM plates.

In this paper it is investigated for the first time how the Unified Formulation by Carrera [41–45,9] can be combined with radial basis functions collocation to the free vibration analysis of thin and thick FG shells, using a higher-order shear deformation theory (HSDT), allowing for through-the-thickness deformations. The effect of $\epsilon_{zz} \neq 0$ in these problems is also investigated. The quality of the present method in predicting free vibrations of thin and thick FG shells is demonstrated through numerical examples.

## 2 The Unified Formulation applied to shell HSDT

The Unified Formulation (UF) proposed by Carrera has been applied in several finite element analysis of beams, plates, and shells, either using the Principle of Virtual Displacements, or by using the Reissner's Mixed Variational theorem. The stiffness matrix components, the external force terms or the inertia terms can be obtained directly with this UF, irrespective of the shear deformation theory being considered. We present in the following the details of the formulation.

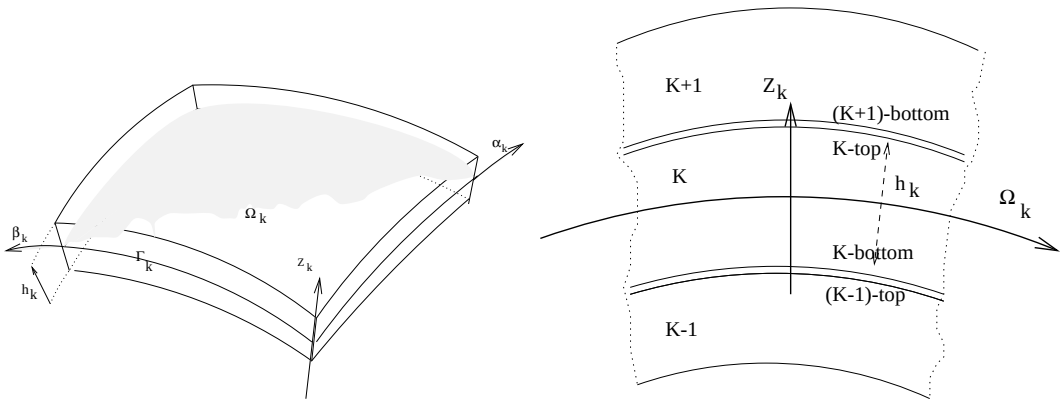


Fig. 1. Geometry and notations for a multilayered shell (doubly curved).

### *2.1 Shell geometry*

Shells are bi-dimensional structures in which one dimension (in general the thickness in $z$ direction) is negligible with respect to the other two in-plane dimensions. The CUF formulation applied to FGM shells considers virtual (mathematical) layers of constant thickness. The geometry and the reference system are indicated in Fig. (1).

### *2.2 A higher-order shear deformation theory*

The present higher-order shear deformation theory involves the following expansion of displacements

$$u(\alpha,\beta,z,t) = u_0(\alpha,\beta,t) + zu_1(\alpha,\beta,t) + z^3u_3(\alpha,\beta,t) \tag{1}$$

$$v(\alpha,\beta,z,t) = v_0(\alpha,\beta,t) + zv_1(\alpha,\beta,t) + z^3v_3(\alpha,\beta,t) \tag{2}$$

$$w(\alpha,\beta,z,t) = w_0(\alpha,\beta,t) + zw_1(\alpha,\beta,t) + z^2w_2(\alpha,\beta,t) \tag{3}$$

where $u$, $v$, and $w$ are the displacements in the $\alpha-$, $\beta-$, and $z-$ directions, respectively. $u_0$, $u_1$, $u_3$, $v_0$, $v_1$, $v_3$, $w_0$, $w_1$, and $w_2$ are functions to be determined. $u_0, v_0$ and $w_0$ are translations of a point at the middle-surface of the shell, and $u_1, v_1, u_3, v_3$ denote rotations. The consideration of higher-order terms in $w$ allows the study of the thickness-stretching effects.

### *2.3 Governing equations and boundary conditions*

The functionally graded shell is divided into a number ($NL$) of uniform thickness layers. The square of an infinitesimal linear segment in the $k$-th layer, the

associated infinitesimal area and volume are given by:

$$
\begin{aligned}
ds_k^2 &= \; H_\alpha^{k\,2}\, d\alpha^2 \; + \; H_\beta^{k\,2}\, d\beta^2 + H_z^{k\,2}\, dz^2 \; , \\
d\Omega_k &= H_\alpha^k H_\beta^k \, d\alpha \, d\beta \; , \\
dV_k &= \; H_\alpha^k \, H_\beta^k \, H_z^k \, d\alpha \, d\beta \, dz \; ,
\end{aligned}
\tag{4}
$$

where the metric coefficients are:

$$
H_\alpha^k = A^k(1 + z/R_\alpha^k), \quad H_\beta^k = B^k(1 + z/R_\beta^k), \quad H_z^k = 1 \; . \tag{5}
$$

$k$ denotes the $k$-layer of the multilayered shell; $R_\alpha^k$ and $R_\beta^k$ are the principal radii of curvature along the coordinates $\alpha$ and $\beta$ respectively. $A^k$ and $B^k$ are the coefficients of the first fundamental form of $\Omega_k$ ($\Gamma_k$ is the $\Omega_k$ boundary). In this work, the attention has been restricted to shells with constant radii of curvature (cylindrical, spherical, toroidal geometries) for which $A^k = B^k = 1$.

The Principle of Virtual Displacements (PVD) for the pure-mechanical case can be expressed as:

$$
\sum_{k=1}^{NL} \int_{\Omega_k} \int_{A_k} \left\{ \delta {\epsilon_{pG}^k}^T \sigma_{pC}^k + \delta {\epsilon_{nG}^k}^T \sigma_{nC}^k \right\} d\Omega_k dz = \sum_{k=1}^{NL} \delta L_e^k \tag{6}
$$

where $\Omega_k$ and $A_k$ are the integration domains in plane ($\alpha$,$\beta$) and $z$ direction, respectively. Here, $k$ indicates the layer and $T$ the transpose of a vector. $G$ means geometrical relations and $C$ constitutive equations and $\delta L_e^k$ is the external work for the $k$th layer.

Stresses and strains are separated into in-plane and normal components, denoted respectively by the subscripts $p$ and $n$. The mechanical strains in the $k$th layer can be related to the displacement field $\boldsymbol{u}^k = \{u_\alpha^k, u_\beta^k, u_z^k\}$ via the geometrical relations:

$$
\epsilon_{pG}^k = [\epsilon_{\alpha\alpha}^k, \epsilon_{\beta\beta}^k, \epsilon_{\alpha\beta}^k]^T = (\boldsymbol{D}_p^k + \boldsymbol{A}_p^k)\, \boldsymbol{u}^k \; , \; \epsilon_{nG}^k = [\epsilon_{\alpha z}^k, \epsilon_{\beta z}^k, \epsilon_{zz}^k]^T = (\boldsymbol{D}_{n\Omega}^k + \boldsymbol{D}_{nz}^k - \boldsymbol{A}_n^k)\, \boldsymbol{u}^k \tag{7}
$$

The explicit form of the introduced arrays follows:

$$
\boldsymbol{D}_p^k = \begin{bmatrix} \frac{\partial_\alpha}{H_\alpha^k} & 0 & 0 \\ 0 & \frac{\partial_\beta}{H_\beta^k} & 0 \\ \frac{\partial_\beta}{H_\beta^k} & \frac{\partial_\alpha}{H_\alpha^k} & 0 \end{bmatrix}, \quad \boldsymbol{D}_{n\Omega}^k = \begin{bmatrix} 0 & 0 & \frac{\partial_\alpha}{H_\alpha^k} \\ 0 & 0 & \frac{\partial_\beta}{H_\beta^k} \\ 0 & 0 & 0 \end{bmatrix}, \quad \boldsymbol{D}_{nz}^k = \begin{bmatrix} \partial_z & 0 & 0 \\ 0 & \partial_z & 0 \\ 0 & 0 & \partial_z \end{bmatrix}, \tag{8}
$$

$$\boldsymbol{A}_p^k = \begin{bmatrix} 0 & 0 & \frac{1}{H_\alpha^k R_\alpha^k} \\ 0 & 0 & \frac{1}{H_\beta^k R_\beta^k} \\ 0 & 0 & 0 \end{bmatrix}, \quad \boldsymbol{A}_n^k = \begin{bmatrix} \frac{1}{H_\alpha^k R_\alpha^k} & 0 & 0 \\ 0 & \frac{1}{H_\beta^k R_\beta^k} & 0 \\ 0 & 0 & 0 \end{bmatrix}. \tag{9}$$

The 3D constitutive equations are given as:

$$\begin{aligned} \sigma_{pC}^k &= \mathbf{C}_{pp}^k \, \epsilon_{pG}^k + \mathbf{C}_{pn}^k \, \epsilon_{nG}^k \\ \sigma_{nC}^k &= \mathbf{C}_{np}^k \, \epsilon_{pG}^k + \mathbf{C}_{nn}^k \, \epsilon_{nG}^k \end{aligned} \tag{10}$$

In the case of functionally graded materials, the matrices $\mathbf{C}_{pp}^k$, $\mathbf{C}_{pn}^k$, $\mathbf{C}_{np}^k$, and $\mathbf{C}_{nn}^k$ are reduced to:

$$\begin{aligned} \mathbf{C}_{pp}^k &= \begin{bmatrix} C_{11}^k & C_{12}^k & 0 \\ C_{12}^k & C_{11}^k & 0 \\ 0 & 0 & C_{44}^k \end{bmatrix} \qquad \mathbf{C}_{pn}^k = \begin{bmatrix} 0 & 0 & C_{12}^k \\ 0 & 0 & C_{12}^k \\ 0 & 0 & 0 \end{bmatrix} \\ \mathbf{C}_{np}^k &= \begin{bmatrix} 0 & 0 & 0 \\ 0 & 0 & 0 \\ C_{12}^k & C_{12}^k & 0 \end{bmatrix} \qquad \mathbf{C}_{nn}^k = \begin{bmatrix} C_{44}^k & 0 & 0 \\ 0 & C_{44}^k & 0 \\ 0 & 0 & C_{33}^k \end{bmatrix} \end{aligned} \tag{11}$$

The computation of elastic constants $C_{ij}^k$ for each layer, considers the following steps:

(1) computation of volume fraction of the ceramic and metal phases
(2) computation of elastic properties $E^k$ and $\nu^k$
(3) computation of elastic constants $C_{ij}$

In the present work, the volume fraction of the ceramic phase is defined according to the power-law:

$$V_c^k = \left(0.5 + \frac{z}{h}\right)^p \tag{12}$$

being $z \in [-h/2, h/2]$, $h$ the thickness of the shell, and the exponent $p$ a scalar parameter that defines gradation of material properties across the thickness direction. The volume fraction of the metal phase is given as $V_m^k = 1 - V_c^k$.

The Young's modulus, $E^k$, and Poisson's ratio, $\nu^k$, are computed by the law-of-mixtures:

$$E^k(z) = E_m V_m^k + E_c V_c^k; \qquad \nu^k(z) = \nu_m V_m^k + \nu_c V_c^k; \tag{13}$$

Then, the computation of the elastic constants $C_{ij}^k$ is performed, depending on the assumption of $\epsilon_{zz}$. If $\epsilon_{zz} = 0$, then $C_{ij}^k$ are the plane-stress reduced elastic constants:

$$C_{11}^k = \frac{E^k}{1-(\nu^k)^2}; \quad C_{12}^k = \nu^k \frac{E^k}{1-(\nu^k)^2}; \quad C_{44}^k = \frac{E^k}{2(1+\nu^k)}; \quad C_{33} = 0 \tag{14}$$

where $E^k$ is the modulus of elasticity, $\nu^k$ is the Poisson's ratio found in previous step.

If $\epsilon_{zz} \neq 0$ (thickness-stretching), then $C_{ij}^k$ are the three-dimensional elastic constants, given by

$$C_{11}^k = \frac{E^k(1-(\nu^k)^2)}{1-3(\nu^k)^2-2(\nu^k)^3}, \quad C_{12}^k = \frac{E^k(\nu^k+(\nu^k)^2)}{1-3(\nu^k)^2-2(\nu^k)^3} \tag{15}$$

$$C_{44}^k = \frac{E^k}{2(1+\nu^k)}, \quad C_{33}^k = \frac{E^k(1-(\nu^k)^2)}{1-3(\nu^k)^2-2(\nu^k)^3} \tag{16}$$

The three displacement components $u_\alpha$, $u_\beta$ and $u_z$ (given in (1) to (3)) and their relative variations can be modelled by CUF as:

$$(u_\alpha, u_\beta, u_z) = F_\tau \, (u_{\alpha\tau}, u_{\beta\tau}, u_{z\tau}) \qquad (\delta u_\alpha, \delta u_\beta, \delta u_z) = F_s \, (\delta u_{\alpha s}, \delta u_{\beta s}, \delta u_{zs}) \tag{17}$$

where $F_\tau$ are functions of the thickness coordinate $z$ and $\tau$ is a sum index. In the present formulation the thickness functions are

$$F_{su\alpha} = F_{su\beta} = F_{\tau u\alpha} = F_{\tau u\beta} = \begin{bmatrix} 1 & z & z^3 \end{bmatrix} \tag{18}$$

for in-plane displacements $u, v$ and

$$F_{sw} = F_{\tau w} = \begin{bmatrix} 1 & z & z^2 \end{bmatrix} \tag{19}$$

for transverse displacement $w$. All the terms of the equations of motion are then obtained by integrating through the thickness direction.

Substituting the geometrical relations, the constitutive equations and the unified formulation into the variational statement PVD, for the $k$th layer, one obtains:

$$\begin{aligned} &\sum_{k=1}^{NL} \{ \int_{\Omega_k} \int_{A_k} \{ ((\boldsymbol{D}_p + \boldsymbol{A}_p)\delta\boldsymbol{u}^k)^T (\boldsymbol{C}_{pp}^k (\boldsymbol{D}_p + \boldsymbol{A}_p)\boldsymbol{u}^k + \boldsymbol{C}_{pn}^k (\boldsymbol{D}_{n\Omega} + \boldsymbol{D}_{nz} - \boldsymbol{A}_n)\boldsymbol{u}^k) + \\ &((\boldsymbol{D}_{n\Omega} + \boldsymbol{D}_{nz} - \boldsymbol{A}_n)\delta\boldsymbol{u}^k)^T (\boldsymbol{C}_{np}^k (\boldsymbol{D}_p + \boldsymbol{A}_p)\boldsymbol{u}^k + \boldsymbol{C}_{nn}^k (\boldsymbol{D}_{n\Omega} + \boldsymbol{D}_{nz} - \boldsymbol{A}_n)\boldsymbol{u}^k) \} d\Omega_k dz_k \} \\ &= \sum_{k=1}^{NL} \delta L_e^k \end{aligned} \tag{20}$$

At this point, the formula of integration by parts is applied:

$$\int_{\Omega_k} \left((\mathbf{D}_\Omega)\delta\mathbf{a}^k\right)^T \mathbf{a}^k d\Omega_k = -\int_{\Omega_k} \delta\mathbf{a}^{kT} \left((\mathbf{D}_\Omega^T)\mathbf{a}^k\right) d\Omega_k + \int_{\Gamma_k} \delta\mathbf{a}^{kT} \left((\mathbf{I}_\Omega)\mathbf{a}^k\right) d\Gamma_k \tag{21}$$

where $\mathbf{I}_\Omega$ matrix is obtained applying the *Divergence theorem*:

$$\int_\Omega \frac{\partial\psi}{\partial x_i} d\upsilon = \oint_\Gamma n_i \psi ds \tag{22}$$

being $n_i$ the components of the normal $\widehat{n}$ to the boundary along the direction $i$. After integration by parts and the substitution of CUF, the governing equations and boundary conditions for the shell in the mechanical case are obtained:

$$\begin{aligned}
&\sum_{k=1}^{NL}\{\int_{\Omega_k}\int_{A_k}\{\delta\boldsymbol{u}_s^{kT}[(-\boldsymbol{D}_p+\boldsymbol{A}_p)^T F_s(\boldsymbol{C}_{pp}^k(\boldsymbol{D}_p+\boldsymbol{A}_p)F_\tau\boldsymbol{u}_\tau^k+\boldsymbol{C}_{pn}^k(\boldsymbol{D}_{n\Omega}+\boldsymbol{D}_{nz}-\boldsymbol{A}_n)F_\tau\boldsymbol{u}_\tau^k)]+\\
&\delta\boldsymbol{u}_s^{kT}[(-\boldsymbol{D}_{n\Omega}+\boldsymbol{D}_{nz}-\boldsymbol{A}_n)^T F_s(\boldsymbol{C}_{np}^k(\boldsymbol{D}_p+\boldsymbol{A}_p)F_\tau\boldsymbol{u}_\tau^k+\boldsymbol{C}_{nn}^k(\boldsymbol{D}_{n\Omega}+\boldsymbol{D}_{nz}-\boldsymbol{A}_n)F_\tau\boldsymbol{u}_\tau^k)]\}d\Omega_k dz_k\}\\
&+\sum_{k=1}^{NL}\{\int_{\Gamma_k}\int_{A_k}\{\delta\boldsymbol{u}_s^{kT}[\boldsymbol{I}_p^T F_s(\boldsymbol{C}_{pp}^k(\boldsymbol{D}_p+\boldsymbol{A}_p)F_\tau\boldsymbol{u}_\tau^k+\boldsymbol{C}_{pn}^k(\boldsymbol{D}_{n\Omega}+\boldsymbol{D}_{nz}-\boldsymbol{A}_n)F_\tau\boldsymbol{u}_\tau^k)]+\\
&\delta\boldsymbol{u}_s^{kT}[\boldsymbol{I}_{np}^T F_s(\boldsymbol{C}_{np}^k(\boldsymbol{D}_p-\boldsymbol{A}_p)F_\tau\boldsymbol{u}_\tau^k+\boldsymbol{C}_{nn}^k(\boldsymbol{D}_{n\Omega}+\boldsymbol{D}_{nz}-\boldsymbol{A}_n)F_\tau\boldsymbol{u}_\tau^k)]\}d\Gamma_k dz_k\}\\
&=\sum_{k=1}^{NL}\{\int_{\Omega_k}\delta\boldsymbol{u}_s^{kT}F_s\boldsymbol{p}_u^k\}\ .
\end{aligned} \tag{23}$$

where $\mathbf{I}_p^k$ and $\mathbf{I}_{np}^k$ depend on the boundary geometry:

$$\mathbf{I}_p=\begin{bmatrix}\frac{n_\alpha}{H_\alpha} & 0 & 0\\ 0 & \frac{n_\beta}{H_\beta} & 0\\ \frac{n_\beta}{H_\beta} & \frac{n_\alpha}{H_\alpha} & 0\end{bmatrix};\mathbf{I}_{np}=\begin{bmatrix}0 & 0 & \frac{n_\alpha}{H_\alpha}\\ 0 & 0 & \frac{n_\beta}{H_\beta}\\ 0 & 0 & 0\end{bmatrix};. \tag{24}$$

The normal to the boundary of domain $\Omega$ is:

$$\widehat{\boldsymbol{n}}=\begin{bmatrix}n_\alpha\\ n_\beta\end{bmatrix}=\begin{bmatrix}cos(\varphi_\alpha)\\ cos(\varphi_\beta)\end{bmatrix} \tag{25}$$

where $\varphi_\alpha$ and $\varphi_\beta$ are the angles between the normal $\widehat{n}$ and the direction $\alpha$ and $\beta$ respectively.

The governing equations for a multi-layered shell subjected to mechanical loadings are:

$$\delta \mathbf{u}_s^{k^T} \; : \qquad \mathbf{K}_{uu}^{k\tau s}\, \mathbf{u}_\tau^k \;=\; \mathbf{P}_{u\tau}^k \tag{26}$$

where the fundamental nucleus $\mathbf{K}_{uu}^{k\tau s}$ is obtained as:

$$\begin{aligned}\boldsymbol{K}_{uu}^{k\tau s} = \int_{A_k} \Big[ &[-\boldsymbol{D}_p + \boldsymbol{A}_p]^T\, \boldsymbol{C}_{pp}^k [\boldsymbol{D}_p + \boldsymbol{A}_p] + [-\boldsymbol{D}_p + \boldsymbol{A}_p]^T\, \boldsymbol{C}_{pn}^k [\boldsymbol{D}_{n\Omega} + \boldsymbol{D}_{nz} - \boldsymbol{A}_n] + \\ &[-\boldsymbol{D}_{n\Omega} + \boldsymbol{D}_{nz} - \boldsymbol{A}_n]^T\, \boldsymbol{C}_{np}^k [\boldsymbol{D}_p + \boldsymbol{A}_p] + [-\boldsymbol{D}_{n\Omega} + \boldsymbol{D}_{nz} - \boldsymbol{A}_n]^T\, \boldsymbol{C}_{nn}^k [\boldsymbol{D}_{n\Omega} + \boldsymbol{D}_{nz} - \boldsymbol{A}_n] \Big] \\ &F_\tau F_s H_\alpha^k H_\beta^k \; dz \; .\end{aligned} \tag{27}$$

and the corresponding Neumann-type boundary conditions on $\Gamma_k$ are:

$$\mathbf{\Pi}_d^{k\tau s}\, \mathbf{u}_\tau^k \;=\; \mathbf{\Pi}_d^{k\tau s}\, \bar{\mathbf{u}}_\tau^k \; , \tag{28}$$

where:

$$\begin{aligned}\mathbf{\Pi}_d^{k\tau s} = \int_{A_k} \Big[ &\boldsymbol{I}_p^T\, \boldsymbol{C}_{pp}^k [\boldsymbol{D}_p + \boldsymbol{A}_p^\tau] + \boldsymbol{I}_p^T\, \boldsymbol{C}_{pn}^k [\boldsymbol{D}_{n\Omega} + \boldsymbol{D}_{nz} - \boldsymbol{A}_n^\tau] + \\ &\boldsymbol{I}_{np}^T \boldsymbol{C}_{np}^k [\boldsymbol{D}_p + \boldsymbol{A}_p^\tau] + \boldsymbol{I}_{np}^T\, \boldsymbol{C}_{nn}^k [\boldsymbol{D}_{n\Omega} + \boldsymbol{D}_{nz} - \boldsymbol{A}_n^\tau] \Big] F_\tau F_s H_\alpha^k H_\beta^k \; dz \; .\end{aligned} \tag{29}$$

and $\mathbf{P}_{u\tau}^k$ are variationally consistent loads with applied pressure.

*2.4 Fundamental nuclei*

The fundamental nucleo $\mathbf{K}_{uu}^{k\tau s}$ is reported for functionally graded doubly curved shells (radii of curvature in both $\alpha$ and $\beta$ directions (see Fig.1)):

$$
\begin{aligned}
\left(\mathbf{K}_{uu}^{\tau sk}\right)_{11} &= -C_{11}^{k} J_{\beta/\alpha}^{k\tau s}\partial_{\alpha}^{s}\partial_{\alpha}^{\tau} - C_{44}^{k} J_{\alpha/\beta}^{k\tau s}\partial_{\beta}^{s}\partial_{\beta}^{\tau} \\
&\quad + C_{44}^{k}\left(J_{\alpha\beta}^{k\tau_z s_z} - \frac{1}{R_{\alpha_k}} J_{\beta}^{k\tau_z s} - \frac{1}{R_{\alpha_k}} J_{\beta}^{k\tau s_z} + \frac{1}{R_{\alpha_k}^{2}} J_{\beta/\alpha}^{k\tau s}\right) \\
\left(\mathbf{K}_{uu}^{\tau sk}\right)_{12} &= -C_{12}^{k} J^{k\tau s}\partial_{\alpha}^{\tau}\partial_{\beta}^{s} - C_{44}^{k} J^{k\tau s}\partial_{\alpha}^{s}\partial_{\beta}^{\tau} \\
\left(\mathbf{K}_{uu}^{\tau sk}\right)_{13} &= -C_{11}^{k}\frac{1}{R_{\alpha_k}} J_{\beta/\alpha}^{k\tau s}\partial_{\alpha}^{\tau} - C_{12}^{k}\frac{1}{R_{\beta_k}} J^{k\tau s}\partial_{\alpha}^{\tau} - C_{12}^{k} J_{\beta}^{k\tau s_z}\partial_{\alpha}^{\tau} \\
&\quad + C_{44}^{k}\left(J_{\beta}^{k\tau_z s}\partial_{\alpha}^{s} - \frac{1}{R_{\alpha_k}} J_{\beta/\alpha}^{k\tau s}\partial_{\alpha}^{s}\right) \\
\left(\mathbf{K}_{uu}^{\tau sk}\right)_{21} &= -C_{12}^{k} J^{k\tau s}\partial_{\alpha}^{s}\partial_{\beta}^{\tau} - C_{44}^{k} J^{k\tau s}\partial_{\alpha}^{\tau}\partial_{\beta}^{s} \\
\left(\mathbf{K}_{uu}^{\tau sk}\right)_{22} &= -C_{22}^{k} J_{\alpha/\beta}^{k\tau s}\partial_{\beta}^{s}\partial_{\beta}^{\tau} - C_{26}^{k} J^{k\tau s}\partial_{\alpha}^{s}\partial_{\beta}^{\tau} - C_{26}^{k} J^{k\tau s}\partial_{\alpha}^{\tau}\partial_{\beta}^{s} - C_{44}^{k} J_{\beta/\alpha}^{k\tau s}\partial_{\alpha}^{s}\partial_{\alpha}^{\tau} \\
&\quad + C_{44}^{k}\left(J_{\alpha\beta}^{k\tau_z s_z} - \frac{1}{R_{\beta_k}} J_{\alpha}^{k\tau_z s} - \frac{1}{R_{\beta_k}} J_{\alpha}^{k\tau s_z} + \frac{1}{R_{\beta_k}^{2}} J_{\alpha/\beta}^{k\tau s}\right) \\
\left(\mathbf{K}_{uu}^{\tau sk}\right)_{23} &= -C_{12}^{k}\frac{1}{R_{\alpha_k}} J^{k\tau s}\partial_{\beta}^{\tau} - C_{22}^{k}\frac{1}{R_{\beta_k}} J_{\alpha/\beta}^{k\tau s}\partial_{\beta}^{\tau} - C_{12}^{k} J_{\alpha}^{k\tau s_z}\partial_{\beta}^{\tau} \\
&\quad + C_{44}^{k}\left(J_{\alpha}^{k\tau_z s}\partial_{\beta}^{s} - \frac{1}{R_{\beta_k}} J_{\alpha/\beta}^{k\tau s}\partial_{\beta}^{s}\right) \\
\left(\mathbf{K}_{uu}^{\tau sk}\right)_{31} &= C_{11}^{k}\frac{1}{R_{\alpha_k}} J_{\beta/\alpha}^{k\tau s}\partial_{\alpha}^{s} + C_{12}^{k}\frac{1}{R_{\beta_k}} J^{k\tau s}\partial_{\alpha}^{s} + C_{12}^{k} J_{\beta}^{k\tau_z s}\partial_{\alpha}^{s} \\
&\quad - C_{44}^{k}\left(J_{\beta}^{k\tau s_z}\partial_{\alpha}^{\tau} - \frac{1}{R_{\alpha_k}} J_{\beta/\alpha}^{k\tau s}\partial_{\alpha}^{\tau}\right) \\
\left(\mathbf{K}_{uu}^{\tau sk}\right)_{32} &= C_{12}^{k}\frac{1}{R_{\alpha_k}} J^{k\tau s}\partial_{\beta}^{s} + C_{22}^{k}\frac{1}{R_{\beta_k}} J_{\alpha/\beta}^{k\tau s}\partial_{\beta}^{s} + C_{12}^{k} J_{\alpha}^{k\tau_z s}\partial_{\beta}^{s} \\
&\quad - C_{44}^{k}\left(J_{\alpha}^{k\tau s_z}\partial_{\beta}^{\tau} - \frac{1}{R_{\beta_k}} J_{\alpha/\beta}^{k\tau s}\partial_{\beta}^{\tau}\right) \\
\left(\mathbf{K}_{uu}^{\tau sk}\right)_{33} &= C_{11}^{k}\frac{1}{R_{\alpha_k}^{2}} J_{\beta/\alpha}^{k\tau s} + C_{22}^{k}\frac{1}{R_{\beta_k}^{2}} J_{\alpha/\beta}^{k\tau s} + C_{33}^{k} J_{\alpha\beta}^{k\tau_z s_z} \\
&\quad + 2C_{12}^{k}\frac{1}{R_{\alpha_k}}\frac{1}{R_{\beta_k}} J^{k\tau s} + C_{12}^{k}\frac{1}{R_{\alpha_k}}\left(J_{\beta}^{k\tau_z s} + J_{\beta}^{k\tau s_z}\right) + C_{12}^{k}\frac{1}{R_{\beta_k}}\left(J_{\alpha}^{k\tau_z s} + J_{\alpha}^{k\tau s_z}\right) \\
&\quad - C_{44}^{k} J_{\alpha/\beta}^{k\tau s}\partial_{\beta}^{s}\partial_{\beta}^{\tau} - C_{44}^{k} J_{\beta/\alpha}^{k\tau s}\partial_{\alpha}^{s}\partial_{\alpha}^{\tau}
\end{aligned}
\tag{30}
$$

where

$$
\begin{aligned}
(J^{k\tau s}, J^{k\tau s}_{\alpha}, J^{k\tau s}_{\beta}, J^{k\tau s}_{\frac{\alpha}{\beta}}, J^{k\tau s}_{\frac{\beta}{\alpha}}, J^{k\tau s}_{\alpha\beta}) &= \int_{A_k} F_\tau F_s(1, H_\alpha, H_\beta, \frac{H_\alpha}{H_\beta}, \frac{H_\beta}{H_\alpha}, H_\alpha H_\beta)\ dz \\
(J^{k\tau_z s}, J^{k\tau_z s}_{\alpha}, J^{k\tau_z s}_{\beta}, J^{k\tau_z s}_{\frac{\alpha}{\beta}}, J^{k\tau_z s}_{\frac{\beta}{\alpha}}, J^{k\tau_z s}_{\alpha\beta}) &= \int_{A_k} \frac{\partial F_\tau}{\partial z} F_s(1, H_\alpha, H_\beta, \frac{H_\alpha}{H_\beta}, \frac{H_\beta}{H_\alpha}, H_\alpha H_\beta)\ dz \\
(J^{k\tau s_z}, J^{k\tau s_z}_{\alpha}, J^{k\tau s_z}_{\beta}, J^{k\tau s_z}_{\frac{\alpha}{\beta}}, J^{k\tau s_z}_{\frac{\beta}{\alpha}}, J^{k\tau s_z}_{\alpha\beta}) &= \int_{A_k} F_\tau \frac{\partial F_s}{\partial z}(1, H_\alpha, H_\beta, \frac{H_\alpha}{H_\beta}, \frac{H_\beta}{H_\alpha}, H_\alpha H_\beta)\ dz \\
(J^{k\tau_z s_z}, J^{k\tau_z s_z}_{\alpha}, J^{k\tau_z s_z}_{\beta}, J^{k\tau_z s_z}_{\frac{\alpha}{\beta}}, J^{k\tau_z s_z}_{\frac{\beta}{\alpha}}, J^{k\tau_z s_z}_{\alpha\beta}) &= \int_{A_k} \frac{\partial F_\tau}{\partial z}\frac{\partial F_s}{\partial z}(1, H_\alpha, H_\beta, \frac{H_\alpha}{H_\beta}, \frac{H_\beta}{H_\alpha}, H_\alpha H_\beta)\ dz
\end{aligned}
\tag{31}
$$

The application of boundary conditions makes use of the fundamental nucleo $\mathbf{\Pi}_d$ in the form:

$$
\begin{aligned}
\left(\mathbf{\Pi}^{\tau sk}_{uu}\right)_{11} &= n_\alpha C^k_{11} J^{k\tau s}_{\beta/\alpha}\partial^s_\alpha + n_\beta C^k_{44} J^{k\tau s}_{\alpha/\beta}\partial^s_\beta \\
\left(\mathbf{\Pi}^{\tau sk}_{uu}\right)_{12} &= n_\alpha C^k_{12} J^{k\tau s}\partial^s_\beta + n_\beta C^k_{44} J^{k\tau s}\partial^s_\alpha \\
\left(\mathbf{\Pi}^{\tau sk}_{uu}\right)_{13} &= n_\alpha \frac{1}{R_{\alpha k}} C^k_{11} J^{k\tau s}_{\beta/\alpha} + n_\alpha \frac{1}{R_{\beta k}} C^k_{12} J^{k\tau s} + n_\alpha C^k_{12} J^{k\tau s_z}_{\beta} \\
\left(\mathbf{\Pi}^{\tau sk}_{uu}\right)_{21} &= n_\beta C^k_{12} J^{k\tau s}\partial^s_\alpha + n_\alpha C^k_{44} J^{k\tau s}\partial^s_\beta \\
\left(\mathbf{\Pi}^{\tau sk}_{uu}\right)_{22} &= n_\alpha C^k_{44} J^{k\tau s}_{\beta/\alpha}\partial^s_\alpha + n_\beta C^k_{22} J^{k\tau s}_{\alpha/\beta}\partial^s_\beta + n_\beta C^k_{26} J^{k\tau s}\partial^s_\alpha + n_\alpha C^k_{26} J^{k\tau s}\partial^s_\beta \\
\left(\mathbf{\Pi}^{\tau sk}_{uu}\right)_{23} &= n_\beta \frac{1}{R_{\alpha k}} C^k_{12} J^{k\tau s} + n_\beta \frac{1}{R_{\beta k}} C^k_{22} J^{k\tau s}_{\alpha/\beta} + n_\beta C^k_{12} J^{k\tau s_z}_{\alpha} \\
\left(\mathbf{\Pi}^{\tau sk}_{uu}\right)_{31} &= -n_\alpha \frac{1}{R_{\alpha k}} C^k_{44} J^{k\tau s}_{\beta/\alpha} + n_\alpha C^k_{44} J^{k\tau s_z}_{\beta} \\
\left(\mathbf{\Pi}^{\tau sk}_{uu}\right)_{32} &= -n_\beta \frac{1}{R_{\beta k}} C^k_{44} J^{k\tau s}_{\alpha/\beta} + n_\beta C^k_{44} J^{k\tau s_z}_{\alpha} \\
\left(\mathbf{\Pi}^{\tau sk}_{uu}\right)_{33} &= n_\alpha C^k_{44} J^{k\tau s}_{\beta/\alpha}\partial^s_\alpha + n_\beta C^k_{44} J^{k\tau s}_{\alpha/\beta}\partial^s_\beta
\end{aligned}
\tag{32}
$$

Note that all the equations written for the shell degenerate in those for the plate when $\frac{1}{R_{\alpha k}} = \frac{1}{R_{\beta k}} = 0$. In practice, the radii of curvature are set to $10^9$ for analysis of plates with the present formulation.

The PVD for the dynamic case is expressed as:

$$\sum_{k=1}^{NL} \int_{\Omega_k} \int_{A_k} \left\{ \delta {\epsilon_{pG}^k}^T \sigma_{pC}^k + \delta {\epsilon_{nG}^k}^T \sigma_{nC}^k \right\} d\Omega_k dz = \sum_{k=1}^{NL} \int_{\Omega_k} \int_{A_k} \rho^k \delta \mathbf{u}^{kT} \ddot{\mathbf{u}}^k d\Omega_k dz + \sum_{k=1}^{NL} \delta L_e^k \tag{33}$$

where $\rho^k$ is the mass density of the $k$-th layer and double dots denote acceleration.

By substituting the geometrical relations and the constitutive equations, one obtains the following governing equations:

$$\delta {\mathbf{u}_s^k}^T \; : \qquad \mathbf{K}_{uu}^{k\tau s} \, \mathbf{u}_\tau^k \, = \mathbf{M}^{k\tau s} \ddot{\mathbf{u}}_\tau^k + \, \mathbf{P}_{u\tau}^k \tag{34}$$

In the case of free vibrations one has:

$$\delta {\mathbf{u}_s^k}^T \; : \qquad \mathbf{K}_{uu}^{k\tau s} \, \mathbf{u}_\tau^k \, = \mathbf{M}^{k\tau s} \ddot{\mathbf{u}}_\tau^k \tag{35}$$

where $\mathbf{M}^{k\tau s}$ is the fundamental nucleus for the inertial term, given by

$$\begin{aligned} \mathbf{M}_{ij}^{k\tau s} &= \rho^k J_{\alpha\beta}^{k\tau s}, \quad i = j \\ \mathbf{M}_{ij}^{k\tau s} &= 0, \quad i \neq j \end{aligned} \tag{36}$$

The meaning of the integral $J_{\alpha\beta}^{k\tau s}$ has been illustrated in eq. (31). The geometrical and mechanical boundary conditions are the same of the static case.

## 3 The radial basis function method for free vibration problems

Consider a linear elliptic partial differential operator $\mathcal{L}$ acting in a bounded region $\Omega$ in $\mathbb{R}^n$ and another operator $\mathcal{L}_B$ acting on a boundary $\partial\Omega$. The eigenproblem looks for eigenvalues ($\lambda$) and eigenvectors ($\mathbf{u}$) that satisfy

$$\mathcal{L}\mathbf{u} + \lambda \mathbf{u} = 0 \text{ in } \Omega \tag{37}$$

$$\mathcal{L}_B \mathbf{u} = 0 \text{ on } \partial\Omega \tag{38}$$

The eigenproblem defined in (37) and (38) will be replaced by a finite-dimensional eigenvalue problem, after the radial basis approximations.

The radial basis function ($\phi$) approximation of a function ($\mathbf{u}$) is given by

$$\tilde{\mathbf{u}}(\mathbf{x}) = \sum_{i=1}^{N} \alpha_i \phi\left(\|x - y_i\|_2\right), \mathbf{x} \in \mathbb{R}^n \tag{39}$$

where $y_i, i = 1, .., N$ is a finite set of distinct points (centers) in $\mathbb{R}^n$.

Derivatives of $\tilde{\mathbf{u}}$ are computed as

$$\frac{\partial \tilde{\mathbf{u}}}{\partial x} = \sum_{j=1}^{N} \alpha_j \frac{\partial \phi_j}{\partial x} \tag{40}$$

$$\frac{\partial^2 \tilde{\mathbf{u}}}{\partial x^2} = \sum_{j=1}^{N} \alpha_j \frac{\partial^2 \phi_j}{\partial x^2}, \text{etc} \tag{41}$$

In the present collocation approach, one needs to impose essential and natural boundary conditions. Consider, for example, the condition $w = 0$, on a simply supported or clamped edge. The conditions are enforced by interpolating as

$$w = 0 \rightarrow \sum_{j=1}^{N} \alpha_j^W \phi_j = 0 \tag{42}$$

Other boundary conditions are interpolated in a similar way.

Examples of some common RBFs are

$$\begin{aligned}
\text{Cubic:} \quad & \phi(r) = r^3 \\
\text{Thin plate splines:} \quad & \phi(r) = r^2 \log(r) \\
\text{Wendland functions:} \quad & \phi(r) = (1-r)_+^m p(r) \\
\text{Gaussian:} \quad & \phi(r) = e^{-(cr)^2} \\
\text{Multiquadrics:} \quad & \phi(r) = \sqrt{c^2 + r^2} \\
\text{Inverse Multiquadrics:} \quad & \phi(r) = (c^2 + r^2)^{-1/2}
\end{aligned}$$

where the Euclidian distance $r$ is real and non-negative and $c$ is a positive shape parameter. Considering $N$ distinct interpolations, and knowing $u(x_j), j = 1, 2, ..., N$, one finds $\alpha_i$ by the solution of a $N \times N$ linear system

$$\mathbf{A}\boldsymbol{\alpha} = \mathbf{u} \tag{43}$$

where $\mathbf{A} = \left[\phi\left(\|x - y_i\|_2\right)\right]_{N \times N}$, $\boldsymbol{\alpha} = [\alpha_1, \alpha_2, ..., \alpha_N]^T$ and $\mathbf{u} = [u(x_1), u(x_2), ..., u(x_N)]^T$.

The solution of the eigenproblem by radial basis functions considers $N_I$ nodes in the interior of the domain and $N_B$ nodes on the boundary, witha total

number of nodes $N = N_I + N_B$. The interpolation points are denoted by $x_i \in \Omega, i = 1, ..., N_I$ and $x_i \in \partial\Omega, i = N_I + 1, ..., N$. At the points in the domain, the following eigenproblem is defined

$$\sum_{i=1}^{N} \alpha_i \mathcal{L}\phi\left(\|x - y_i\|_2\right) = \lambda \tilde{\mathbf{u}}(x_j), j = 1, 2, ..., N_I \tag{44}$$

or

$$\mathcal{L}^I \boldsymbol{\alpha} = \lambda \tilde{\mathbf{u}}^I \tag{45}$$

where

$$\mathcal{L}^I = \left[\mathcal{L}\phi\left(\|x - y_i\|_2\right)\right]_{N_I \times N} \tag{46}$$

At the points on the boundary, the imposed boundary conditions are

$$\sum_{i=1}^{N} \alpha_i \mathcal{L}_B \phi\left(\|x - y_i\|_2\right) = 0, j = N_I + 1, ..., N \tag{47}$$

or

$$\mathbf{B}\boldsymbol{\alpha} = 0 \tag{48}$$

where $\mathbf{B} = \mathcal{L}_B \phi\left[\left(\|x_{N_I+1} - y_j\|_2\right)\right]_{N_B \times N}$.

Therefore, one can write a finite-dimensional eigenvalue problem and solve equations (45) and (48) as a generalized eigenvalue problem

$$\begin{bmatrix} \mathcal{L}^I \\ \mathbf{B} \end{bmatrix} \boldsymbol{\alpha} = \lambda \begin{bmatrix} \mathbf{A}^I \\ \mathbf{0} \end{bmatrix} \boldsymbol{\alpha} \tag{49}$$

where

$$\mathbf{A}^I = \phi\left[\left(\|x_{N_I} - y_j\|_2\right)\right]_{N_I \times N}$$

For free vibration problems an harmonic solution is assumed for the displacements $u_0, u_1, v_0, v_1, \cdots$

$$\begin{aligned} u_0 &= U_0(x,y)e^{i\omega t}; \quad u_1 = U_1(x,y)e^{i\omega t}; \quad u_3 = U_3(x,y)e^{i\omega t} \\ v_0 &= V_0(x,y)e^{i\omega t}; \quad v_1 = V_1(x,y)e^{i\omega t}; \quad v_3 = V_3(x,y)e^{i\omega t} \\ w_0 &= W_0(x,y)e^{i\omega t}; \quad w_1 = W_1(x,y)e^{i\omega t}; \quad w_2 = W_2(x,y)e^{i\omega t} \end{aligned} \tag{50}$$

where $\omega$ is the frequency of natural vibration. Substituting the harmonic expansion into equations (49) in terms of the amplitudes $U_0, U_1, U_3, V_0, V_1, V_3, W_0, W_1, W_2$, one can obtain the natural frequencies and vibration modes for the plate or shell problem, by solving the eigenproblem

$$\left[\mathcal{L} - \omega^2 \mathcal{G}\right] \mathbf{X} = \mathbf{0} \tag{51}$$

where $\mathcal{L}$ collects all stiffness terms and $\mathcal{G}$ collects all terms related to the inertial terms. In (51) $\mathbf{X}$ are the modes of vibration associated with the natural frequencies defined as $\omega$.

## 4 Numerical results

In this section the higher-order shear deformation theory is combined with radial basis functions collocation for the free vibration analysis of functionally graded shell panels. Examples include spherical ($R_x = R_y = R$) as well as cylindrical ($R_x = R$ and $R_y = \infty$) shell panels with all edges clamped (CCCC) or simply supported (SSSS). Particular cases of these are also considered: isotropic materials (fully ceramic, $p = 0$, and fully metal, $p = \infty$) and plates ($R_x = R_y = \infty$).

To study the effect of $\epsilon_{zz} \neq 0$ in these problems, the case $\epsilon_{zz} = 0$ is implemented by considering $w = w_0$ instead (3).

Results are compared with those from Pradyumna and Bandyopadhyay [46], who used finite elements formulation and a HSDT disregarding through-the-thickness deformations.

The following material properties are used:

silicon nitride ($Si_3N_4$):

$$E_c = 322.2715GPa,\ \nu_c = 0.24,\ \rho_c = 2370Kg/m^3 \tag{52}$$

stainless steel ($SUS304$):

$$E_m = 207.7877GPa,\ \nu_m = 0.31776,\ \rho_m = 8166Kg/m^3 \tag{53}$$

aluminum:

$$E_m = 70GPa,\ \nu_m = 0.3,\ \rho_m = 2707Kg/m^3 \tag{54}$$

alumina:

$$E_c = 380GPa,\ \nu_c = 0.3,\ \rho_c = 3000Kg/m^3 \tag{55}$$

The non-dimensional frequency is given as

$$\bar{w} = wa^2\sqrt{\frac{\rho_m h}{D}} \quad \text{where} \quad D = \frac{E_m h^3}{12(1-\nu_m^2)}. \tag{56}$$

In all numerical examples a Chebyshev grid is employed (see figure 2) and the

| grid | $13^2$ | $17^2$ | $19^2$ | $21^2$ |
|---|---|---|---|---|
| $1^{st}$ | 60.3483 | 60.3431 | 60.3499 | 60.3479 |
| $2^{nd}$ | 115.2450 | 115.2134 | 115.2315 | 115.2044 |
| $3^{rd}$ | 115.3917 | 115.3665 | 115.3755 | 115.3347 |
| $4^{th}$ | 162.1741 | 162.0337 | 162.0727 | 162.0860 |

Table 1
Initial study. Square CCCC FG cylindrical panel, $Si_3N_4$ and $SUS304$, $a/h = 10$, $a/R = 0.1$, $p = 0.2$.

Wendland function defined as

$$\phi(r) = (1 - c\ r)_+^8 \left(32(c\ r)^3 + 25(c\ r)^2 + 8c\ r + 1\right) \tag{57}$$

Here, the shape parameter ($c$) is obtained by an optimization procedure, as detailed in Ferreira and Fasshauer [47].

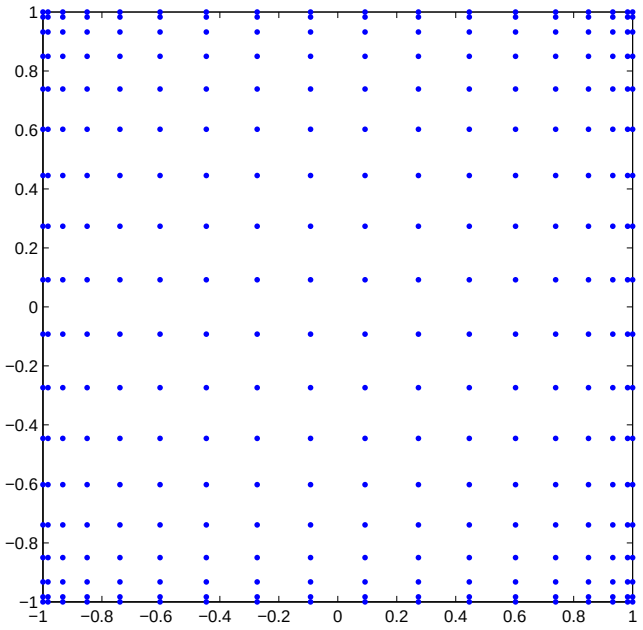


Fig. 2. A sketch of a Chebyshev grid for $17^2$ points

An initial study was performed to show the convergence of the present approach and select the number of points to use in the computation of the vibration problems. Results are presented in table 1 and refer to the first four vibration modes of a clamped functionally graded cylindrical shell panel composed of silicon nitride (52) and stainless steel (53), with side-to-thickness ratio $a/h = 10$, side-to-radius ratio $a/R = 0.1$, power law exponent $p = 0.2$, and $a = b = 2$. A $17^2$ grid was chosen for the following vibration problems.

| mode | source | $p=0$ ($Si_3N_4$) | $p=0.2$ | $p=2$ | $p=10$ | $p=\infty$ ($SUS304$) |
|---|---|---|---|---|---|---|
| 1 | ref. [46] | 72.9613 | 60.0269 | 39.1457 | 33.3666 | 32.0274 |
| | ref. [48] | 74.518 | 57.479 | 40.750 | 35.852 | 32.761 |
| | present $\epsilon_{zz}=0$ | 74.2634 | 60.0061 | 40.5259 | 35.1663 | 32.6108 |
| | present $\epsilon_{zz}\neq 0$ | 74.5821 | 60.3431 | 40.8262 | 35.4229 | 32.8593 |
| 2 | ref. [46] | 138.5552 | 113.8806 | 74.2915 | 63.2869 | 60.5546 |
| | ref. [48] | 144.663 | 111.717 | 78.817 | 69.075 | 63.314 |
| | present $\epsilon_{zz}=0$ | 141.6779 | 114.3788 | 76.9725 | 66.6482 | 61.9329 |
| | present $\epsilon_{zz}\neq 0$ | 142.4281 | 115.2134 | 77.6639 | 67.1883 | 62.4886 |
| 3 | ref. [46] | 138.5552 | 114.0266 | 74.3868 | 63.3668 | 60.6302 |
| | ref. [48] | 145.740 | 112.531 | 79.407 | 69.609 | 63.806 |
| | present $\epsilon_{zz}=0$ | 141.8485 | 114.5495 | 77.0818 | 66.7332 | 62.0082 |
| | present $\epsilon_{zz}\neq 0$ | 142.6024 | 115.3665 | 77.7541 | 67.2689 | 62.5668 |
| 4 | ref. [46] | 195.5366 | 160.6235 | 104.7687 | 89.1970 | 85.1788 |
| | ref. [48] | 206.992 | 159.855 | 112.457 | 98.386 | 90.370 |
| | present $\epsilon_{zz}=0$ | 199.1566 | 160.7355 | 107.9484 | 93.3350 | 86.8160 |
| | present $\epsilon_{zz}\neq 0$ | 200.3158 | 162.0337 | 108.9677 | 94.0923 | 87.6341 |

Table 2
First 4 modes of a CCCC square FG cylindrical shell panel, $Si_3N_4$ and $SUS304$, $a/h=10$, $a/R=0.1$, for several $p$.

### *4.1 Clamped functionally graded cylindrical shell panel*

The free vibration of clamped FG cylindrical shell panels is analysed.

In table 2 the first 4 vibration modes of a square clamped FG cylindrical shell panel with constituents silicon nitride (52) and stainless steel (53), side-to-thickness ratio $a/h=10$, side-to-radius ratio $a/R=0.1$, and several power law exponents $p$ are presented. Results are compared with [46] and those from Yang and Shen [48], with the differential quadrature approximation and Galerkin technique, both neglecting through-the-thickness deformations.

In figure 3 the first 4 modes of a CCCC square FG cylindrical shell panel, with constituents silicon nitride and stainless steel, ratios $a/h=10$ and $R/a=10$, and power law exponent $p=0.2$ are presented.

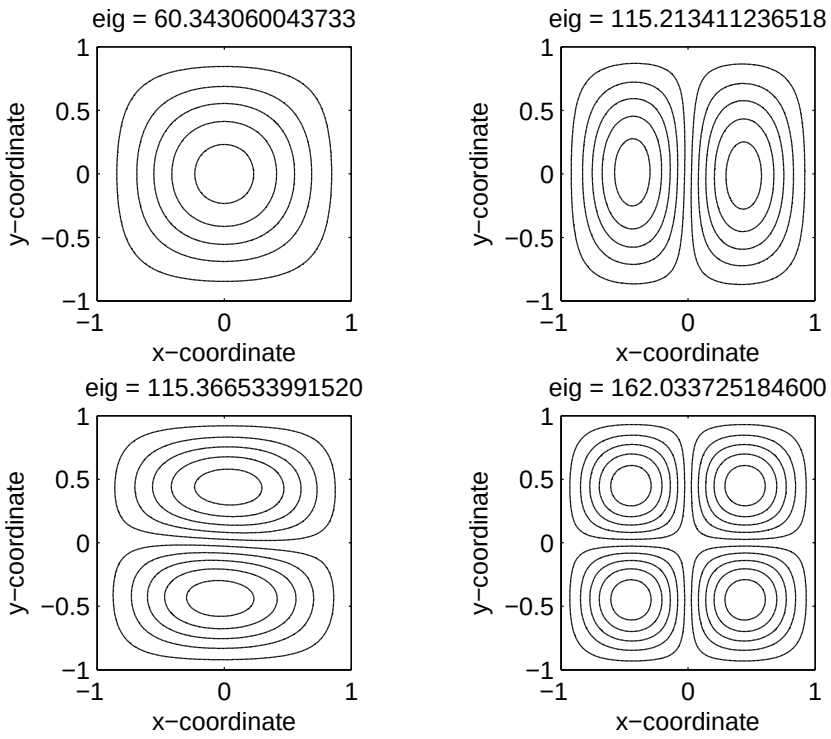


Fig. 3. First 4 modes of a CCCC square FG cylindrical shell panel, $Si_3N_4$ and $SUS304$, $a/h = 10$, $a/R = 0.1$, $p = 0.2$.

The fundamental frequency of square clamped FG cylindrical shell panels composed of aluminum (54) and alumina (55), with side-to-radius ratio $a/R = 0.1$, various side-to-thickness ratios $a/h$ and power law exponents $p$ are presented in table 3.

The results of the present approach in tables 2 and 3 compare well with references. The combination of present HSDT and the meshless technique based on collocation with radial basis function shows very good accuracy in the free vibration analysis of FG shells.

In table 4 the fundamental frequency of square clamped FG cylindrical shell panels composed of aluminum (54) and alumina (55), with side-to-thickness ratios $a/h = 10$, are presented considering various side-to-radius ratio $a/R$, and power law exponents $p$.

### *4.2 Simply supported functionally graded cylindrical shell panel*

The free vibration of simply supported FG cylindrical shell panels is now analysed.

| $p$ | source | $a/h$ =5 | $a/h$ =10 | $a/h$ =15 | $a/h$ =20 | $a/h$ =50 | $a/h$ =100 |
|---|---|---|---|---|---|---|---|
| 0 | FSDT | 56.5548 | 70.8035 | 75.7838 | 77.5654 | 85.4346 | 103.4855 |
| | ref. [46] | 58.2858 | 71.7395 | 75.0439 | 77.0246 | 84.8800 | 102.9227 |
| | present $\epsilon_{zz} = 0$ | 59.0433 | 72.3272 | 76.4904 | 78.4918 | 85.6073 | 102.3351 |
| | present $\epsilon_{zz} \neq 0$ | 59.7741 | 72.8141 | 76.8148 | 78.7342 | 85.7713 | 102.7871 |
| 0.5 | FSDT | 47.2468 | 57.7597 | 62.2838 | 63.8393 | 70.3199 | 87.1049 |
| | ref. [46] | 48.7185 | 58.5305 | 61.5835 | 63.1381 | 69.8604 | 86.5452 |
| | present $\epsilon_{zz} = 0$ | 49.3050 | 59.5188 | 62.6780 | 64.2371 | 70.4237 | 85.4780 |
| | present $\epsilon_{zz} \neq 0$ | 49.9508 | 59.9353 | 62.9544 | 64.4438 | 70.5664 | 85.9029 |
| 1 | FSDT | 42.0305 | 51.0884 | 55.4209 | 56.7991 | 62.8458 | 77.7762 |
| | ref. [46] | 43.4243 | 52.0173 | 54.7015 | 56.0880 | 62.2152 | 77.0774 |
| | present $\epsilon_{zz} = 0$ | 43.9548 | 52.8776 | 55.6437 | 57.0255 | 62.7088 | 76.6386 |
| | present $\epsilon_{zz} \neq 0$ | 44.5754 | 53.2759 | 55.9081 | 57.2226 | 62.8414 | 77.0381 |

Table 3
Fundamental frequencies of CCCC square FG cylindrical shell panels composed of aluminum and alumina, $R/a = 0.1$, for various $a/h$ and $p$.

Table 5 presents the fundamental frequency of a square simply supported FG cylindrical shell panel with constituents aluminum (54) and alumina (55), length-to-thickness ratio $a/h = 10$, and several length-to-radius ratio $a/R$ and several power law exponents $p$ as well.

In figure 4 the relationships between fundamental frequency and the radius-to-length ratio $R/a$ is visualized for various power law exponents $p$. It refers to the square simply supported FG cylindrical shell panel composed from aluminum (54) and alumina (55), with side-to-thickness ratio $a/h = 10$. The graphic on the left was obtained from tabulated values on table 5 and the right one is more detailed for values of $p$ smaller or equal than 5 ($p = 0.5, 1, 2, 3, 4, 5$).

### *4.3 Clamped functionally graded spherical shell panel*

We now study the free vibration of clamped FG spherical shell panels.

The fundamental frequency of a square clamped FG spherical shell panel with constituents aluminum (54) and alumina (55), and side-to-thickness ratio $a/h = 10$, considering various side-to-radius ratios $a/R$, and several power law exponents $p$ are presented in table 6.

| $p$ | source | $R/a$ =0.5 | $R/a$ =1 | $R/a$ =5 | $R/a$ =10 | $R/a$ =50 | Plate |
|---|---|---|---|---|---|---|---|
| 0 | ref. [46] | 129.9808 | 94.4973 | 71.8861 | 71.0394 | 70.7660 | 70.7546 |
| | present $\epsilon_{zz} = 0$ | 133.6037 | 95.5849 | 73.1640 | 72.3304 | 72.0614 | 72.0502 |
| | present $\epsilon_{zz} \neq 0$ | 134.5056 | 96.0131 | 73.6436 | 72.8141 | 72.5465 | 72.5353 |
| 0.2 | ref. [46] | 119.6109 | 87.3930 | 68.1152 | 67.3320 | 67.0801 | 67.0698 |
| | present $\epsilon_{zz} = 0$ | 121.8612 | 87.8148 | 66.6620 | 65.8808 | 65.6371 | 65.6299 |
| | present $\epsilon_{zz} \neq 0$ | 122.7375 | 88.1659 | 67.1004 | 66.3235 | 66.0814 | 66.0743 |
| 0.5 | ref. [46] | 108.1546 | 79.5689 | 63.1896 | 62.4687 | 62.2380 | 62.2291 |
| | present $\epsilon_{zz} = 0$ | 110.2017 | 80.0146 | 60.2477 | 59.5215 | 59.3022 | 59.2985 |
| | present $\epsilon_{zz} \neq 0$ | 111.0739 | 80.3049 | 60.6568 | 59.9353 | 59.7178 | 59.7142 |
| 1 | ref. [46] | 96.0666 | 71.2453 | 56.5546 | 55.8911 | 55.6799 | 55.6722 |
| | present $\epsilon_{zz} = 0$ | 97.9069 | 71.6716 | 53.5430 | 52.8800 | 52.6864 | 52.6856 |
| | present $\epsilon_{zz} \neq 0$ | 98.7955 | 71.9167 | 53.9340 | 53.2759 | 53.0841 | 53.0835 |
| 2 | ref. [46] | 84.4431 | 62.9748 | 36.2487 | 35.6633 | 35.4745 | 35.4669 |
| | present $\epsilon_{zz} = 0$ | 86.3088 | 63.4398 | 47.5205 | 46.9447 | 46.7820 | 46.7835 |
| | present $\epsilon_{zz} \neq 0$ | 87.2271 | 63.6675 | 47.9060 | 47.3343 | 47.1726 | 47.1741 |
| 10 | ref. [46] | 69.8224 | 51.3803 | 33.6611 | 33.1474 | 32.9812 | 32.9743 |
| | present $\epsilon_{zz} = 0$ | 71.7634 | 52.0900 | 40.8099 | 40.4145 | 40.3028 | 40.3037 |
| | present $\epsilon_{zz} \neq 0$ | 72.3922 | 52.2780 | 41.0985 | 40.7046 | 40.5923 | 40.5929 |
| $\infty$ | ref. [46] | 61.0568 | 44.2962 | 32.4802 | 32.0976 | 31.9741 | 31.9689 |
| | present $\epsilon_{zz} = 0$ | 60.3660 | 43.1880 | 33.0576 | 32.6810 | 32.5594 | 32.5543 |
| | present $\epsilon_{zz} \neq 0$ | 60.7735 | 43.3815 | 33.2743 | 32.8995 | 32.7786 | 32.7735 |

Table 4
Fundamental frequencies of CCCC square FG cylindrical shell panels composed of aluminum and alumina, $a/h = 10$, for various $R/a$ and $p$.

### *4.4 Simply supported functionally graded spherical shell panel*

This example considers the free vibration of simply supported FG spherical shell panels.

The fundamental frequency of a square simply supported FG spherical shell panel composed of aluminum (54) and alumina (55), with side-to-thickness ratio $a/h = 10$, are presented in table 7 considering various side-to-radius ratios $a/R$ as well power law exponents $p$.

| $p$ | source | $R/a$ =0.5 | $R/a$ =1 | $R/a$ =5 | $R/a$ =10 | $R/a$ =50 | Plate |
|---|---|---|---|---|---|---|---|
| 0 | ref. [46] | 68.8645 | 51.5216 | 42.2543 | 41.9080 | 41.7963 | 41.7917 |
| | present $\epsilon_{zz} = 0$ | 70.1594 | 52.1938 | 42.6701 | 42.3153 | 42.2008 | 42.1961 |
| | present $\epsilon_{zz} \neq 0$ | 69.9872 | 52.1101 | 42.7172 | 42.3684 | 42.2560 | 42.2513 |
| 0.2 | ref. [46] | 64.4001 | 47.5968 | 40.1621 | 39.8472 | 39.7465 | 39.7426 |
| | present $\epsilon_{zz} = 0$ | 65.3889 | 47.9338 | 38.7168 | 38.3840 | 38.2842 | 38.2827 |
| | present $\epsilon_{zz} \neq 0$ | 65.2100 | 47.8590 | 38.7646 | 38.4368 | 38.3384 | 38.3368 |
| 0.5 | ref. [46] | 59.4396 | 43.3019 | 37.2870 | 36.9995 | 36.9088 | 36.9057 |
| | present $\epsilon_{zz} = 0$ | 60.4255 | 43.6883 | 34.8768 | 34.5672 | 34.4809 | 34.4820 |
| | present $\epsilon_{zz} \neq 0$ | 60.2422 | 43.6239 | 34.9273 | 34.6219 | 34.5365 | 34.5376 |
| 1 | ref. [46] | 53.9296 | 38.7715 | 33.2268 | 32.9585 | 32.8750 | 32.8726 |
| | present $\epsilon_{zz} = 0$ | 54.8909 | 39.1753 | 30.9306 | 30.6485 | 30.5759 | 30.5792 |
| | present $\epsilon_{zz} \neq 0$ | 54.7074 | 39.1246 | 30.9865 | 30.7077 | 30.6355 | 30.6386 |
| 2 | ref. [46] | 47.8259 | 34.3338 | 27.4449 | 27.1789 | 27.0961 | 27.0937 |
| | present $\epsilon_{zz} = 0$ | 48.7807 | 34.7654 | 27.5362 | 27.2979 | 27.2423 | 27.2472 |
| | present $\epsilon_{zz} \neq 0$ | 48.6005 | 34.7289 | 27.5977 | 27.3616 | 27.3055 | 27.3102 |
| 10 | ref. [46] | 37.2593 | 28.2757 | 19.3892 | 19.1562 | 19.0809 | 19.0778 |
| | present $\epsilon_{zz} = 0$ | 38.2792 | 28.8072 | 24.2472 | 24.1063 | 24.0762 | 24.0802 |
| | present $\epsilon_{zz} \neq 0$ | 38.1172 | 28.7611 | 24.2839 | 24.1444 | 24.1125 | 24.1171 |
| $\infty$ | ref. [46] | 31.9866 | 24.1988 | 19.0917 | 18.9352 | 18.8848 | 18.8827 |
| | present $\epsilon_{zz} = 0$ | 31.7000 | 23.5827 | 19.2796 | 19.1193 | 19.0675 | 19.0654 |
| | present $\epsilon_{zz} \neq 0$ | 31.6222 | 23.5448 | 19.3008 | 19.1433 | 19.0924 | 19.0903 |

Table 5
Fundamental frequencies of SSSS square FG cylindrical shell panels composed of aluminum and alumina, $a/h = 10$, for various $R/a$ and $p$.

### *4.5 Discussion*

All results presented in tables 2 to 7 are in excellent agreement with references considered. Exceptions are $p = 10$ and $R/a = 5, 10, 50$ for the SSSS panels, and $p = 2, 10$ and $R/a = 5, 10, 50$ for the CCCC panels. The authors did not find any explanation for these exceptions.

A detailed analysis of previous tables lead us to the following conclusions:

- **Boundary conditions:** Clamped FG shell panels present higher frequency

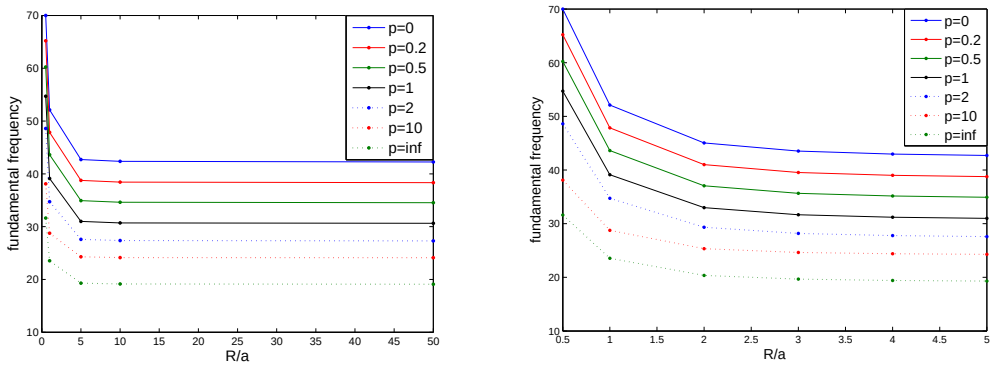


Fig. 4. Fundamental frequency as a function of the radius-to-length ratio for several $p$.

values than simply supported ones.

- **Geometry:** Lower radii of curvature values present higher frequency values, i. e., the fundamental frequency decreases as the ratio $R/a$ increases.
- **Material properties:** The fundamental frequency of FG shell panels decreases as the exponent $p$ in power-law increases.

Another conclusion from all tables, as easily seen in figure 4, is that the fundamental frequency decreases as the radius of curvature increases. The fall-off is faster for smaller values of $R$ ($R/a$) and then shows fast convergence.

The effect of $\epsilon_{zz} \neq 0$ shows significance in thicker shells (see table 2) and seems independent of the radius of curvature (see tables 4 to 7 ).

## 5 Concluding remarks

For the first time, Carrera's Unified Formulation was combined with the radial basis functions collocation technique for the free vibration analysis of functionally graded shells. A higher-order shear deformation theory that allows extensibility in the thickness direction was implemented and the effect of $\epsilon_{zz} \neq 0$ was studied.

Numerical results were compared with other sources and the present approach demonstrated to be successful in the free vibration analysis of functionally graded shells and easy to implement.

| $p$ | source | $R/a$ =0.5 | $R/a$ =1 | $R/a$ =5 | $R/a$ =10 | $R/a$ =50 | Plate |
|---|---|---|---|---|---|---|---|
| 0 | ref. [46] | 173.9595 | 120.9210 | 73.5550 | 71.4659 | 70.7832 | 70.7546 |
| | present $\epsilon_{zz} = 0$ | 176.8125 | 122.0934 | 74.8207 | 72.7536 | 72.0784 | 72.0502 |
| | present $\epsilon_{zz} \neq 0$ | 176.8356 | 122.3533 | 75.2810 | 73.2322 | 72.5633 | 72.5353 |
| 0.2 | ref. [46] | 161.3704 | 112.2017 | 69.6597 | 67.7257 | 67.0956 | 67.0698 |
| | present $\epsilon_{zz} = 0$ | 163.0852 | 112.7143 | 68.2142 | 66.2686 | 65.6498 | 65.6299 |
| | present $\epsilon_{zz} \neq 0$ | 163.0460 | 112.8132 | 68.6329 | 66.7063 | 66.0938 | 66.0743 |
| 0.5 | ref. [46] | 147.4598 | 102.5983 | 64.6114 | 62.8299 | 62.2519 | 62.2291 |
| | present $\epsilon_{zz} = 0$ | 149.0931 | 103.1804 | 61.6902 | 59.8745 | 59.3112 | 59.2985 |
| | present $\epsilon_{zz} \neq 0$ | 149.0095 | 103.1490 | 62.0789 | 60.2831 | 59.7265 | 59.7142 |
| 1 | ref. [46] | 132.3396 | 92.2147 | 57.8619 | 56.2222 | 55.6923 | 55.6722 |
| | present $\epsilon_{zz} = 0$ | 133.8751 | 92.8282 | 54.8597 | 53.1956 | 52.6921 | 52.6856 |
| | present $\epsilon_{zz} \neq 0$ | 133.7710 | 92.6962 | 55.2302 | 53.5864 | 53.0895 | 53.0835 |
| 2 | ref. [46] | 116.4386 | 81.3963 | 37.3914 | 35.9568 | 35.4861 | 35.4669 |
| | present $\epsilon_{zz} = 0$ | 118.0167 | 82.0948 | 48.6656 | 47.2135 | 46.7849 | 46.7835 |
| | present $\epsilon_{zz} \neq 0$ | 117.9317 | 81.9179 | 49.0328 | 47.5990 | 47.1754 | 47.1741 |
| 10 | ref. [46] | 92.1387 | 64.8773 | 34.6658 | 33.4057 | 32.9916 | 32.9743 |
| | present $\epsilon_{zz} = 0$ | 93.9111 | 65.8103 | 41.6016 | 40.5998 | 40.3049 | 40.3037 |
| | present $\epsilon_{zz} \neq 0$ | 93.8398 | 65.7018 | 41.8796 | 40.8883 | 40.5946 | 40.5929 |
| $\infty$ | ref. [46] | 80.7722 | 56.2999 | 33.2343 | 32.2904 | 31.9819 | 31.9689 |
| | present $\epsilon_{zz} = 0$ | 79.8889 | 55.1653 | 33.8061 | 32.8722 | 32.5671 | 32.5543 |
| | present $\epsilon_{zz} \neq 0$ | 79.8994 | 55.2827 | 34.0141 | 33.0884 | 32.7862 | 32.7735 |

Table 6
Fundamental frequencies of CCCC square FG spherical shell panels composed of aluminum and alumina, $a/h = 10$, for various $R/a$ and $p$.

## 6 Acknowledgement

The first author is grateful for the grant SFRH/BD/45554/2008 assured by FCT.

| $p$ | source | $R/a$ =0.5 | $R/a$ =1 | $R/a$ =5 | $R/a$ =10 | $R/a$ =50 | Plate |
|---|---|---|---|---|---|---|---|
| 0 | ref. [46] | 124.1581 | 78.2306 | 44.0073 | 42.3579 | 41.8145 | 41.7917 |
| | present $\epsilon_{zz} = 0$ | 126.2994 | 79.2626 | 44.4455 | 42.7709 | 42.2192 | 42.1961 |
| | present $\epsilon_{zz} \neq 0$ | 126.0882 | 79.0008 | 44.4697 | 42.8180 | 42.2741 | 42.2513 |
| 0.2 | ref. [46] | 115.7499 | 72.6343 | 41.7782 | 40.2608 | 39.7629 | 39.7426 |
| | present $\epsilon_{zz} = 0$ | 117.3053 | 73.2663 | 40.3936 | 38.8074 | 38.2988 | 38.2827 |
| | present $\epsilon_{zz} \neq 0$ | 117.0197 | 73.0034 | 40.4211 | 38.8551 | 38.3528 | 38.3368 |
| 0.5 | ref. [46] | 106.5014 | 66.5025 | 38.7731 | 37.3785 | 36.9234 | 36.9057 |
| | present $\epsilon_{zz} = 0$ | 108.0044 | 67.1623 | 36.4453 | 34.9574 | 34.4922 | 34.4820 |
| | present $\epsilon_{zz} \neq 0$ | 107.6572 | 66.9033 | 36.4782 | 35.0080 | 34.5478 | 34.5376 |
| 1 | ref. [46] | 96.2587 | 59.8521 | 34.6004 | 33.3080 | 32.8881 | 32.8726 |
| | present $\epsilon_{zz} = 0$ | 97.6938 | 60.5121 | 32.3691 | 31.0012 | 30.5840 | 30.5792 |
| | present $\epsilon_{zz} \neq 0$ | 97.2968 | 60.2636 | 32.4101 | 31.0572 | 30.6437 | 30.6386 |
| 2 | ref. [46] | 84.8206 | 52.7875 | 28.7459 | 27.5110 | 27.1085 | 27.0937 |
| | present $\epsilon_{zz} = 0$ | 86.2288 | 53.4659 | 28.7833 | 27.5984 | 27.2474 | 27.2472 |
| | present $\epsilon_{zz} \neq 0$ | 85.8028 | 53.2311 | 28.8329 | 27.6602 | 27.3109 | 27.3102 |
| 10 | ref. [46] | 65.2296 | 41.6702 | 20.4691 | 19.4357 | 19.0922 | 19.0778 |
| | present $\epsilon_{zz} = 0$ | 66.7088 | 42.4365 | 25.0772 | 24.3034 | 24.0791 | 24.0802 |
| | present $\epsilon_{zz} \neq 0$ | 66.3594 | 42.2155 | 25.1038 | 24.3401 | 24.1168 | 24.1171 |
| $\infty$ | ref. [46] | 57.2005 | 36.2904 | 19.8838 | 19.1385 | 18.8930 | 18.8827 |
| | present $\epsilon_{zz} = 0$ | 57.0657 | 35.8131 | 20.0818 | 19.3251 | 19.0759 | 19.0654 |
| | present $\epsilon_{zz} \neq 0$ | 56.9702 | 35.6948 | 20.0927 | 19.3464 | 19.1006 | 19.0903 |

Table 7
Fundamental frequencies of SSSS square FG spherical shell panels composed of aluminum and alumina, $a/h = 10$, for various $R/a$ and $p$.

## References


[1] M.B. Bever and P.E. Duwez. Gradients in composite materials. *Materials Science and Engineering*, 10(0):1 – 8, 1972.

[2] Y. Miyamoto, W.A. Kaysser, B.H. Rabin, A. Kawasaki, and R.G. Ford. *Functionally Graded Materials: Design, Processing and Applications*. Kluwer Academic Publishers, 1999.

[3] F.J. Ferrante and L.L. Graham-Brady. Stochastic simulation of non-gaussian/non-stationary properties in a functionally graded plate. *Computer*

*Methods in Applied Mechanics and Engineering*, 194(12-16):1675 – 1692, 2005.

[4] H.M Yin, L.Z Sun, and G.H Paulino. Micromechanics-based elastic model for functionally graded materials with particle interactions. *Acta Materialia*, 52(12):3535 – 3543, 2004.

[5] Zheng Zhong and Ertao Shang. Closed-form solutions of three-dimensional functionally graded plates. *Mechanics of Advanced Materials and Structures*, 15(5):355–363, 2008.

[6] T. K. Nguyen, K. Sab, and G. Bonnet. Shear correction factors for functionally graded plates. *Mechanics of Advanced Materials and Structures*, 14(8):567–575, 2007.

[7] Victor Birman and Larry W. Byrd. Modeling and analysis of functionally graded materials and structures. *Applied Mechanics Reviews*, 60(5):195–216, 2007.

[8] M. Koizumi. Fgm activities in japan. *Composites Part B: Engineering*, 28(1-2):1 – 4, 1997. Use of Composites Multi-Phased and Functionally Graded Materials.

[9] E. Carrera. Theories and finite elements for multilayered plates and shells: a unified compact formulation with numerical assessment and benchmarking. *Archives of Computational Methods in Engineering*, 10:215–296, 2003.

[10] D. Chapelle and K.-J. Bathe. *The finite element analysis of shells.-Fundamentals*. Springer, Berlin, 2003.

[11] W. Flügge. *Stresses in shells*. 2nd edn. Springer, Berlin, 1960.

[12] A. Scordelis and K. S. Lo. Computer analysis in cylindrical shells. *Journal of American Concrete Institute*, 61:561–593, 1964.

[13] J. N. Reddy. Bending of laminated anisotropic shells by a shear deformable finite element. *Fibre Science and Technology*, 17:9–24, 1982.

[14] E. J. Kansa. Multiquadrics- a scattered data approximation scheme with applications to computational fluid dynamics. i: Surface approximations and partial derivative estimates. *Computers and Mathematics with Applications*, 19(8/9):127–145, 1990.

[15] Y. C. Hon, M. W. Lu, W. M. Xue, and Y. M. Zhu. Multiquadric method for the numerical solution of byphasic mixture model. *Applied Mathematics and Computation*, 88:153–175, 1997.

[16] Y. C. Hon, K. F. Cheung, X. Z. Mao, and E. J. Kansa. A multiquadric solution for the shallow water equation. *ASCE Journal of Hydraulic Engineering*, 125(5):524–533, 1999.

[17] J. G. Wang, G. R. Liu, and P. Lin. Numerical analysis of biot's consolidation process by radial point interpolation method. *International Journal of Solids and Structures*, 39(6):1557–1573, 2002.

[18] G. R. Liu and Y. T. Gu. A local radial point interpolation method (lrpim) for free vibration analyses of 2-d solids. *Journal of Sound and Vibration*, 246(1):29–46, 2001.

[19] G. R. Liu and J. G. Wang. A point interpolation meshless method based on radial basis functions. *International Journal for Numerical Methods in Engineering*, 54:1623–1648, 2002.

[20] J. G. Wang and G. R. Liu. On the optimal shape parameters of radial basis functions used for 2-d meshless methods. *Computer Methods in Applied Mechanics and Engineering*, 191:2611–2630, 2002.

[21] X. L. Chen, G. R. Liu, and S. P. Lim. An element free galerkin method for the free vibration analysis of composite laminates of complicated shape. *Composite Structures*, 59:279–289, 2003.

[22] K. Y. Dai, G. R. Liu, S. P. Lim, and X. L. Chen. An element free galerkin method for static and free vibration analysis of shear-deformable laminated composite plates. *Journal of Sound and Vibration*, 269:633–652, 2004.

[23] G. R. Liu and X. L. Chen. Buckling of symmetrically laminated composite plates using the element-free galerkin method. *International Journal of Structural Stability and Dynamics*, 2:281–294, 2002.

[24] K. M. Liew, X. L. Chen, and J. N. Reddy. Mesh-free radial basis function method for buckling analysis of non-uniformity loaded arbitrarily shaped shear deformable plates. *Computer Methods in Applied Mechanics and Engineering*, 193:205–225, 2004.

[25] Y. Q Huang and Q. S. Li. Bending and buckling analysis of antisymmetric laminates using the moving least square differential quadrature method. *Computer Methods in Applied Mechanics and Engineering*, 193:3471–3492, 2004.

[26] L. Liu, G. R. Liu, and V. C. B. Tan. Element free method for static and free vibration analysis of spatial thin shell structures. *Computer Methods in Applied Mechanics and Engineering*, 191:5923–5942, 2002.

[27] S. Xiang, K. M. Wang, Y. T. Ai, Y. D. Sha, and H. Shi. Analysis of isotropic, sandwich and laminated plates by a meshless method and various shear deformation theories. *Composite Structures*, 91(1):31–37, 2009.

[28] S. Xiang, H. Shi, K. M. Wang, Y. T. Ai, and Y. D. Sha. Thin plate spline radial basis functions for vibration analysis of clamped laminated composite plates. *European Journal of Mechanics A/Solids*, 29:844–850, 2010.

[29] Ferreira A. J. A. Roque, C. M. C. and R. M. N. Jorge. Analysis of composite and sandwich plate by trigonometric layer-wise deformation theory and radial basis function. *J. Sandwich Struct. Mater.*, 8:497–515, 2006.

[30] A. J. M. Ferreira. A formulation of the multiquadric radial basis function method for the analysis of laminated composite plates. *Composite Structures*, 59:385–392, 2003.

[31] A. J. M. Ferreira. Thick composite beam analysis using a global meshless approximation based on radial basis functions. *Mechanics of Advanced Materials and Structures*, 10:271–284, 2003.

[32] A. J. M. Ferreira, C. M. C. Roque, and P. A. L. S. Martins. Analysis of composite plates using higher-order shear deformation theory and a finite point formulation based on the multiquadric radial basis function method. *Composites: Part B*, 34:627–636, 2003.

[33] A.J.M. Ferreira, C.M.C. Roque, E. Carrera, M. Cinefra, and O. Polit. Radial basis functions collocation and a unified formulation for bending, vibration and buckling analysis of laminated plates, according to a variation of murakamiâĂŹs zig-zag theory. *European Journal of Mechanics - A/Solids*, 30(4):559 – 570, 2011.

[34] J.D. Rodrigues, C.M.C. Roque, A.J.M. Ferreira, E. Carrera, and M. Cinefra. Radial basis functions-finite differences collocation and a unified formulation for bending, vibration and buckling analysis of laminated plates, according to murakami's zig-zag theory. *Composite Structures*, 93(7):1613 – 1620, 2011.

[35] A.J.M. Ferreira, C.M.C. Roque, E. Carrera, and M. Cinefra. Analysis of thick isotropic and cross-ply laminated plates by radial basis functions and a unified formulation. *Journal of Sound and Vibration*, 330(4):771 – 787, 2011.

[36] A. J.M. Ferreira, C. M.C. Roque, E. Carrera, M. Cinefra, and O. Polit. Two higher order zig-zag theories for the accurate analysis of bending, vibration and buckling response of laminated plates by radial basis functions collocation and a unified formulation. *Journal of Composite Materials*, 2011.

[37] A. Ferreira, E. Carrera, M. Cinefra, and C. Roque. Analysis of laminated doubly-curved shells by a layerwise theory and radial basis functions collocation, accounting for through-the-thickness deformations. *Computational Mechanics*, 48:13–25, 2011. 10.1007/s00466-011-0579-4.

[38] A.J.M. Ferreira, E. Carrera, M. Cinefra, C.M.C. Roque, and O. Polit. Analysis of laminated shells by a sinusoidal shear deformation theory and radial basis functions collocation, accounting for through-the-thickness deformations. *Composites Part B: Engineering*, 42(5):1276 – 1284, 2011.

[39] A.M.A. Neves, A.J.M. Ferreira, E. Carrera, C.M.C. Roque, M. Cinefra, R.M.N. Jorge, and C.M.M. Soares. Bending of fgm plates by a sinusoidal plate formulation and collocation with radial basis functions. *Mechanics Research Communications*, 38(5):368 – 371, 2011.

[40] A.M.A. Neves, A.J.M. Ferreira, E. Carrera, C.M.C. Roque, M. Cinefra, R. M.N. Jorge, and C.M.M. Soares. A quasi-3d sinusoidal shear deformation theory for the static and free vibration analysis of functionally graded plates. *Composites Part B*, In Press, Accepted Manuscript:–, 2011.

[41] E. Carrera. Developments, ideas, and evaluations based upon reissner's mixed variational theorem in the modelling of multilayered plates and shells. *Applied Mechanics Reviews*, 54:301–329, 2001.

[42] E. Carrera. On the use of murakami's zig-zag function in the modeling of layered plates and shells. *Compos. Struct.*, 82:541–554, 2004.

[43] E. Carrera and S.Brischetto. Analysis of thickness locking in classical, refined and mixed theories for layered shells. *Composite Structures*, 85:83–90, 2008.

[44] M. Soave M. Cinefra, S. Belouettar and E. Carrera. Variable kinematic models applied to free-vibration analysis of functionally graded material shells. *European Journal of Mechanics A/Solids*, 29:1078–1087, 2010.

[45] B. Kröplin M. D'Ottavio, D. Ballhause and E. Carrera. Closed-form solutions for the free-vibration problem of multilayered piezoelectric shells. *Computers and Structures*, 84:1506–1518, 2006.

[46] S. Pradyumna and J.N. Bandyopadhyay. Free vibration analysis of functionally graded curved panels using a higher-order finite element formulation. *Journal of Sound and Vibration*, 318(1-2):176 – 192, 2008.

[47] A. J. M. Ferreira and G. E. Fasshauer. Computation of natural frequencies of shear deformable beams and plates by a rbf-pseudospectral method. *Computer Methods in Applied Mechanics and Engineering*, 196:134–146, 2006.

[48] J. Yang and Hui-Shen Shen. Free vibration and parametric resonance of shear deformable functionally graded cylindrical panels. *Journal of Sound and Vibration*, 261(5):871 – 893, 2003.